

# New method of particle identification with tracker detectors

Ferenc Siklér

*KFKI Research Institute for Particle and Nuclear Physics, Budapest, Hungary*

---

## Abstract

Tracker detectors can be used to identify charged particles based on their global  $\chi$  value obtained during track fitting with the Kalman filter. This approach builds upon the knowledge of detector material and local position resolution, using the known physics of multiple scattering and energy loss. The proposed method is independent of the traditional way of identification using deposited energy. The performance for present LHC experiments is demonstrated.

*Key words:* Particle identification, Multiple scattering, Energy loss, Tracker detectors

*PACS:* 29.40.Gx, 29.85.-c

---

## 1. Introduction

The momentum of a charged particle can be measured by examining the small angle scatters of the trajectory during propagation through the detector medium or tracker layers. For a recent application see Ref. [1] where the root mean square of the scattering angle distribution is computed for each track and compared to the theoretical estimate which is proportional to  $1/\beta p$ . By assuming particle type, or at high momentum ( $\beta \approx 1$ ),  $p$  can be estimated. This classical method underestimates momentum since the particle loses energy and its momentum decreases.

The Kalman filter is widely used in present particle physics experiments for charged track and vertex fitting and provides a coherent framework to handle known physical effects and measurement uncertainties [2]. It is equivalent to a global linear least-squares fit which takes into account all correlations coming from process noise. It is the optimum solution since it minimizes the mean square estimation error. Recent studies show that this technique can be successfully used to improve momentum resolution of particles, even in experiments without magnetic field [3]. It is possible via the effects of multiple scattering. If the detector is in magnetic field, the momentum of charged particles can be obtained from the bending of the trajectory. Hence track fitting may provide additional information that could constrain the velocity of the particle, thus contributing to particle separation or identification.

This article is organized as follows: Sec. 2 introduces the merit function of a track fit  $\chi$  and discusses its characteristics. Sec. 3 deals with physical effects during track propagation, while in Sec. 4 the basic scaling properties of  $\chi$  are given. In Sec. 5 the details of the Monte Carlo simulation and the obtained performance are shown. This work ends with conclusions and it is supplemented by two Appendices.

## 2. The merit function of the fitted track

There are various merit functions that can characterize the goodness of a track fit: sum of the squared and properly normalized predicted ( $P$ ), filtered ( $F$ ) or smoothed ( $S$ ) residuals. It can be easily shown that for each hit  $\chi_p^2 = \chi_F^2$ . The filtered residuals are uncorrelated and in the Gaussian case independent. Hence  $\sum \chi_F^2$  is chi-square distributed with  $r = [\sum_k \dim(m_k)] - n_p$  degrees of freedom, where  $\dim(m_k)$  is the dimension of the  $k$ th hit on track and  $n_p$  is the number of track parameters.

---

*Email address:* sikler@rmki.kfki.hu (Ferenc Siklér)

Tests with smoothed residuals (e.g. for outlier removal) appear to be more powerful [2], but the correlations of these residuals between the states have to be taken into account. Their global covariance matrix  $\mathcal{R}_{kl}$  between smoothed states  $k$  and  $l$  can be calculated [4] with the recursion

$$C_{k-1,l}^n = A_{k-1} C_{k,l}^n, \quad k \leq l$$

and

$$\mathcal{R}_{kl} = V_k \delta_{kl} - H_k C_{k,l}^n H_l^T$$

where  $C$  is the smoothed covariance matrix,  $A$  is the gain matrix,  $V$  is the covariance of measurement noise,  $H$  is the measurement projection matrix. Here we follow the notations of Refs. [2, 4]. The vector of smoothed residuals is described by a multivariate Gaussian distribution with the global covariance  $\mathcal{R}$  obtained above. Since Kalman filtering consists of a series of linear transformations, the smoothed residuals can be obtained from the predicted ones by a linear transformation  $r_S = B r_P$ . Note that no translation is allowed, since the average of both residuals is zero. The global covariance matrix of predicted residuals is  $\mathcal{R}_P$ , the covariance for  $r_S$  is  $\mathcal{R}_S = B \mathcal{R}_P B^T$ . Thus, the expression for the corrected sum of smoothed values is

$$\begin{aligned} \left( \sum \chi_S^2 \right)' &= r_S^T \mathcal{R}_S^{-1} r_S = (B_P r_P)^T (B_P \mathcal{R}_P B_P^T)^{-1} (B_P r_P) = \\ &= (r_P^T B_P^T) (B_P^T)^{-1} \mathcal{R}_P^{-1} B_P^{-1} (B_P r_P) = r_P^T \mathcal{R}_P^{-1} r_P = \sum \chi_P^2. \end{aligned}$$

It is clear that the correlations are transformed out and we get back simply the predicted or filtered values:  $\sum \chi_P^2 = \sum \chi_S^2 = \left( \sum \chi_S^2 \right)'$ . Hence the most straightforward quantity to calculate is the sum  $\chi^2 \equiv \sum \chi_P^2$  using predicted residuals which will be used in the remaining part of this study.

During track propagation the mass of the tracked particle has to be assumed. In collider experiments it is often set to the mass of the most abundantly produced particle, the pion, or that of the muon. The obtained merit function with mass assumption  $m_0$  is

$$\chi^2(m_0) = \sum_k r_k^T R_k^{-1} r_k$$

where the index  $k$  runs for all the measurements and  $R_k$  is the local covariance matrix for the  $k$ th measurement. If the largest contributions to  $R_k$  are independent in  $r\phi$  and  $z$  directions,  $\chi^2$  can be written as

$$\begin{aligned} \chi^2(m_0) &\approx \sum_i \left( \frac{x_i - \mu_i(m_0)}{\sigma_i(m_0)} \right)^2 = \\ &= \sum_i \left( \frac{\sigma_i(m)}{\sigma_i(m_0)} \right)^2 \left( \frac{x_i - \mu_i(m_0)}{\sigma_i(m)} \right)^2 = \sum_i a_i z_i \quad (1) \end{aligned}$$

where  $i$  runs for all split measurements and  $\sigma_i$  are the corresponding standard deviations. The resulted sum is a linear combination of non-centrally chi-square distributed independent random variables  $z_i$  with weights  $a_i$ . The distribution functions are  $f_X(z_i; 1, \lambda_i)$  where

$$a_i = \left( \frac{\sigma_i(m)}{\sigma_i(m_0)} \right)^2, \quad \lambda_i = \left( \frac{\mu_i(m) - \mu_i(m_0)}{\sigma_i(m)} \right)^2.$$

The sum in Eq. (1) can be approximated by a single rescaled non-central chi-squared distribution  $1/\alpha^2 f_X(x/\alpha^2; r, \lambda^2)$  such that

$$\alpha^2 = \frac{\sum_i a_i^2}{\sum_i a_i}, \quad r = \frac{(\sum_i a_i)^2}{\sum_i a_i^2} - n_p, \quad \lambda^2 = \sum_i \lambda_i$$

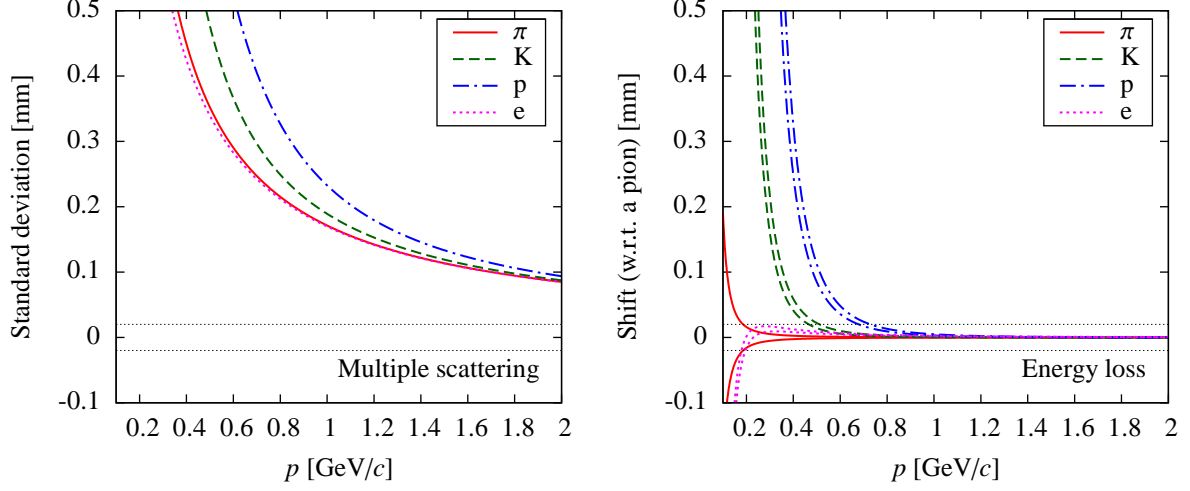


Figure 1: The contributions to deviations and shifts of the predicted hit in a  $B = 3.8$  T magnetic field, after crossing  $x/X_0 = 2\%$  silicon and further  $l = 5$  cm propagation before reaching the next layer, as a function of particle momentum. Left: expected standard deviations due multiple scattering. Right: expected shifts, compared to an average propagation with  $\pi$  mass assumption, due to energy loss. The curves give the limits of the lower and upper  $\pm 1\sigma$  confidence intervals for several particle types. For comparison lines corresponding to a local position resolution of  $25 \mu\text{m}$  are drawn.

where  $n_p$  is the number of track parameters. For details see Appendix B. If  $m = m_0$ , we get  $a_i = 1$ ,  $\alpha = 1$ ,  $\lambda = 0$ , and the distribution is a chi-squared one. If the ratio of expected variances  $a_i$  are similar for all  $i$ , we get

$$\alpha^2 \approx \left\langle \left( \frac{\sigma_i(m)}{\sigma_i(m_0)} \right)^2 \right\rangle \quad (2)$$

and  $r$  is the number of split measurements decreased by the number of track parameters.

At the same time the use of the variable  $\chi \equiv \sqrt{\chi^2}$  appears to be more practical. It is described by a scaled non-central chi-distribution  $1/\alpha f(\chi/\alpha; r, \lambda)$  and well approximated by a Gaussian with parameters

$$\mu_\chi = \alpha \sqrt{r - \frac{1}{2} + \lambda^2}, \quad \sigma_\chi = \alpha \sqrt{\frac{1}{2}}. \quad (3)$$

For detailed derivation see Appendix A.

The value of  $\chi$  can be calculated for each track during the track fit with Kalman filter. For different type of particles it will have different distribution function, because the parameters  $\mu_\chi$  and  $\sigma_\chi$  (via  $\alpha$  and  $r$ ) depend on the ratio of expected hit deviations  $\sigma_i(m)/\sigma_i(m_0)$  which are mass dependent (see Sec. 3). This observation allows to use this quantity in particle identification. Using the Gaussian approximation of Eq. (3), the separation power  $\rho_\chi$  of  $\chi$  between particles of mass  $m_1$  and  $m_2$  is

$$\rho_\chi = \frac{2[\mu_\chi(m_1) - \mu_\chi(m_2)]}{\sqrt{\sigma_\chi^2(m_1) + \sigma_\chi^2(m_2)}}. \quad (4)$$

### 3. Physical effects

When a stable charged particle propagates through material the most important effects which alter its momentum vector are multiple scattering ( $ms$ ) and energy loss ( $el$ ). In the following the expected spatial shift  $\delta$  and deviation  $\sigma$  will be calculated. They are to be compared with the resolution of the local position measurement  $\sigma_{pos}$  of the tracker layers.

The distribution of multiple Coulomb scattering is roughly Gaussian [5], the standard deviation of the planar scattering angle is

$$\theta_0 = \frac{13.6 \text{ MeV}}{\beta c p} z \sqrt{x/X_0} [1 + 0.038 \ln(x/X_0)] \quad (5)$$

where  $p$ ,  $\beta c$ , and  $z$  are the momentum, velocity, and charge of the particle in electron charge units, and  $x/X_0$  is the thickness of the scattering material in radiation lengths. While the expected shift is  $\delta_{ms} = 0$ , the average deviation on the next tracker plane after a flight path  $l$ , in case of normal incidence, is

$$\sigma_{ms} \approx l \theta_0. \quad (6)$$

Momentum and energy is lost during traversal of sensitive detector layers and support structures. To a good approximation the most probable energy loss  $\Delta_p$ , and the full width of the energy loss distribution at half maximum  $\Gamma_\Delta$  [6] are

$$\Delta_p = \xi \left[ \ln \frac{2mc^2 \beta^2 \gamma^2 \xi}{I^2} + 0.2000 - \beta^2 - \delta \right] \quad (7)$$

$$\Gamma_\Delta = 4.018 \xi \quad (8)$$

where

$$\xi = \frac{K}{2} z^2 \frac{Z}{A} \rho \frac{x}{\beta^2}$$

is the Landau parameter;  $K = 4\pi N_A r_e^2 m_e c^2$ ;  $Z$ ,  $A$  and  $\rho$  are the mass number, atomic number and the density of the material, respectively [5]. Since this study deals with momenta below 2 GeV/c, the density correction  $\delta$  was neglected.

In most cases tracker detectors are placed in magnetic field ( $B$ ). Given the radius of the trajectory  $r$  and the length of the arc  $l$ , the central angle is  $\varphi = l/r$ . If the radius is changed by  $\delta r$ , the angle changes by  $\delta\varphi = -l/r^2 \delta r$  and the position shift of the trajectory after  $l$  path is

$$\delta_{el} \approx l \delta\varphi/2 = -l^2/2 \delta r/r^2$$

At the same time  $p = 0.3Br$ ,  $E dE = p dp$ . Hence

$$\delta_{el} \approx -\frac{0.3Bl^2}{2} \frac{\langle \Delta \rangle}{\beta p^2}.$$

Similarly, the expected deviation is

$$\sigma_{el} \approx \frac{0.3Bl^2}{2} \frac{\sigma_\Delta}{\beta p^2}.$$

The contributions to deviations and shifts of the predicted hit in a  $B = 3.8$  T magnetic field, after crossing  $x/X_0 = 2\%$  silicon and further  $l = 5$  cm propagation before reaching the next layer, are shown in Fig. 1. Standard deviations are dominated by multiple scattering, although at very low momentum the energy loss, at very high momentum the local position measurement also plays a role. Shifts from energy loss are only relevant at very low momentum, but they are still very small compared to standard deviations.

#### 4. Properties of $\chi$

It is important to study the sensitivity of the measured  $\chi$  distribution at a given total momentum  $p$ . The parameters which govern the distribution (Eq. (3)) are the rescaler  $\alpha$ , the average shift  $\lambda$  and the number of degrees of freedom  $r$ . In this section we estimate them, as well as the separation power  $\rho_\chi$  listed in Eq. (4), based on physical effects.

Since the deviations are dominated by multiple scattering and local position measurement,  $\alpha$  in Eq. (2) can be approximated as

$$\alpha \approx \sqrt{\frac{\sigma_{ms}^2(m) + \sigma_{pos}^2}{\sigma_{ms}^2(m_0) + \sigma_{pos}^2}}$$

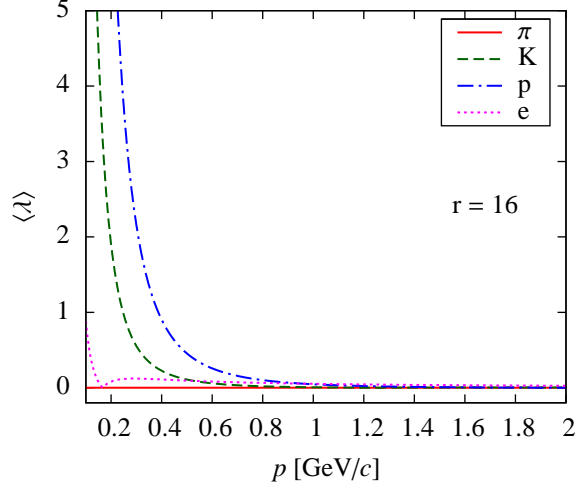


Figure 2: The average shift for several particle types, in a  $B = 3.8$  T magnetic field, with layer thicknesses of  $x/X_0 = 2\%$  silicon, an average propagation length of  $l = 5$  cm, in case of  $r = 16$  number of degrees of freedom, as a function of the particle momentum.

which can be further simplified, if  $\sigma_{pos} \ll \sigma_{ms}$ , to

$$\alpha \approx \frac{\beta(m_0)}{\beta(m)} \left[ 1 - \frac{\zeta^2}{2} \left( 1 - \frac{\beta^2(m)}{\beta^2(m_0)} \right) \right]$$

where the sensitivity is defined as  $\zeta = \sigma_{pos}/\sigma_{ms}(m_0)$ , it is proportional to  $1/\beta p$  (Eqs. (5)–(6)). If the local position resolution can be neglected ( $\zeta \ll 1$ ) we get

$$\alpha \approx \frac{\beta(m_0)}{\beta(m)}. \quad (9)$$

Shifts come entirely from differences in energy loss, hence contributions to  $\lambda$  are only substantial at low momentum:

$$\lambda \approx \sqrt{r} \frac{0.3Bl^2 \langle \Delta(m) - \Delta(m_0) \rangle}{2\beta p^2 l \theta_0} \propto \frac{l \sqrt{rx}}{p} \left( \frac{1}{\beta^2(m)} - \frac{1}{\beta^2(m_0)} \right).$$

The average shift  $\langle \lambda \rangle$  in a  $B = 3.8$  T magnetic field, with layer thicknesses of  $x/X_0 = 2\%$  silicon, an average propagation length of  $l = 5$  cm, in case of  $r = 16$  number of degrees of freedom, is shown in Fig. 2.

If  $\lambda, \zeta \ll 1$ , the separation power  $\rho_\chi$  between particles  $m$  and  $m_0$  is

$$\rho_\chi \approx 2 \sqrt{2r-1} \frac{1 - \beta(m)/\beta(m_0)}{\sqrt{1 + [\beta(m)/\beta(m_0)]^2}}. \quad (10)$$

Hence if the momentum is not very low and the local position resolution is small compared to deviations from multiple scattering, neither the rescaler  $\alpha$  nor the separation power  $\rho_\chi$  depends on the details of the experimental setup, such as magnetic field, radii of tracker layers, value of local position resolution and material thickness. In this respect the only decisive parameter is the number of split measurements which enters the above expressions by the number of degrees of freedom  $r$ . The mean and variance of the corresponding Gaussians are fully determined by the momentum and mass of the particles via  $\beta$ .

Although at low momentum the prediction of the means is more difficult due to the increasing  $\lambda$ , the variances still stay the same. The  $\chi$  distribution can be easily unfolded, since the separation power is large, allowing for a many-parameter fit.

Table 1: Important characteristics of the inner barrel detectors of the studied experimental setup. For details see text at the beginning of Sec. 5.

	$B$ [T]	Subdetector	Radius of layers [cm]	$\sigma_{r\phi}$ [ $\mu\text{m}$ ]	$\sigma_z$ [ $\mu\text{m}$ ]	$x/X_0$ [%]	$\zeta_{r\phi}$	$\zeta_z$	Split meas.
Exp A	2	pixels (barrel)	5.0, 8.8, 12.2	10	115	4	0.1	1	50
		strips (SCT) <sup>s</sup>	29.9, 37.1, 44.3, 51.4	17	580	4	0.1	3	
		straw (TRT)	56.3 – 106.6 ( $\leq 36$ hits)	130	–	0.5	10	–	
Exp B	0.4	pixels (SPD)	3.9, 7.6	12	100	1	0.2	2	12
		drifts (SDD)	14.9, 23.8	35	23	1	0.3	0.2	
		strips (SSD) <sup>s</sup>	38.5, 43.6	15	730	1	0.1	7	
		[gas (TPC)]	84.5 – 246.6 ( $\leq 159$ hits)	900	900	$10^{-3}$	$10^3 - 10^4$	–	
Exp C	3.8	pixels (PXB)	4.4, 7.3, 10.2	15	15	3	0.2	0.2	20
		strips (TIB) <sup>s</sup>	25.5, 33.9	$23/\sqrt{2}$	230	4	0.1	0.8	
		strips (TIB)	41.8, 49.8	35	–	2	0.2	–	
		strips (TOB) <sup>s</sup>	60.8, 69.2	$53/\sqrt{2}$	530	4	0.1	2	
		strips (TOB)	78.0, 86.8, 96.5, 108.0	53, 35	–	2	0.2	–	

#### 4.1. Applications

The measured value of  $\chi$  is sensitive to the proper spatial alignment of the detector layers and to the correct estimate of the variation of the predicted local position. If the alignment precision is sufficient, the latter is mostly determined by the contribution from multiple scattering which is closely proportional to  $\sqrt{x/X_0}$ . While  $p$  and  $r$  are well measured, the amount of material in the detector can be

- *understood*: the unfolding of the  $\chi$  distribution in a phase space bin enables the measurement of yields of different particle species.
- *poorly known*: the unfolding of the  $\chi$  distribution in a phase space bin may provide corrections to the material thickness. They can be extracted by fitting the  $\chi$  distribution with an additional rescaler. Note that the measurement of yields of different particle species is still possible, although with lower confidence.

## 5. Simulation

The proposed method was verified by a Monte Carlo simulation. As examples from LHC, the performance of simplified models for the inner detectors of the following experiments were studied:

- ATLAS (Exp A): three layers of silicon pixels, five layers of double-sided silicon strips, up to 36 layers of straw tubes [7].
- ALICE (Exp B): two layers of silicon pixels, two layers of silicon drifts and two layers of double-sided silicon strips [8, 9]. Due to the large  $\zeta$  value of the gas detector (TPC) its measurements were not included.
- CMS (Exp C): three layers of silicon pixels, ten layers of silicon strips (four of them double-sided) [10].

Some relevant details of the experimental setups are given in Table 1. For simplicity a homogeneous longitudinal magnetic field was used, and detector layers were assumed to be concentric cylinders around the beam-line. Pixels, double-sided strips (superscript <sup>s</sup>), drift layers and gas provide measurements in two dimensions ( $r\phi$  and  $z$ ), while one-sided strips and straw tubes give only measurement in one direction ( $r\phi$ ).  $x/X_0$  values are given per layer and they are rounded to integers where possible. Sensitivity values  $\zeta_{r\phi}$  and  $\zeta_z$  are shown for pions at  $p = 1$  GeV/ $c$ , normal incidence, rounded to one significant digit. The number of split measurements are also indicated.

The initial state vector was estimated by fitting a helix to the first three hits. (These hits are two-dimensional in all three examined experimental setups.) The starting values of the track parameters were extracted at the closest

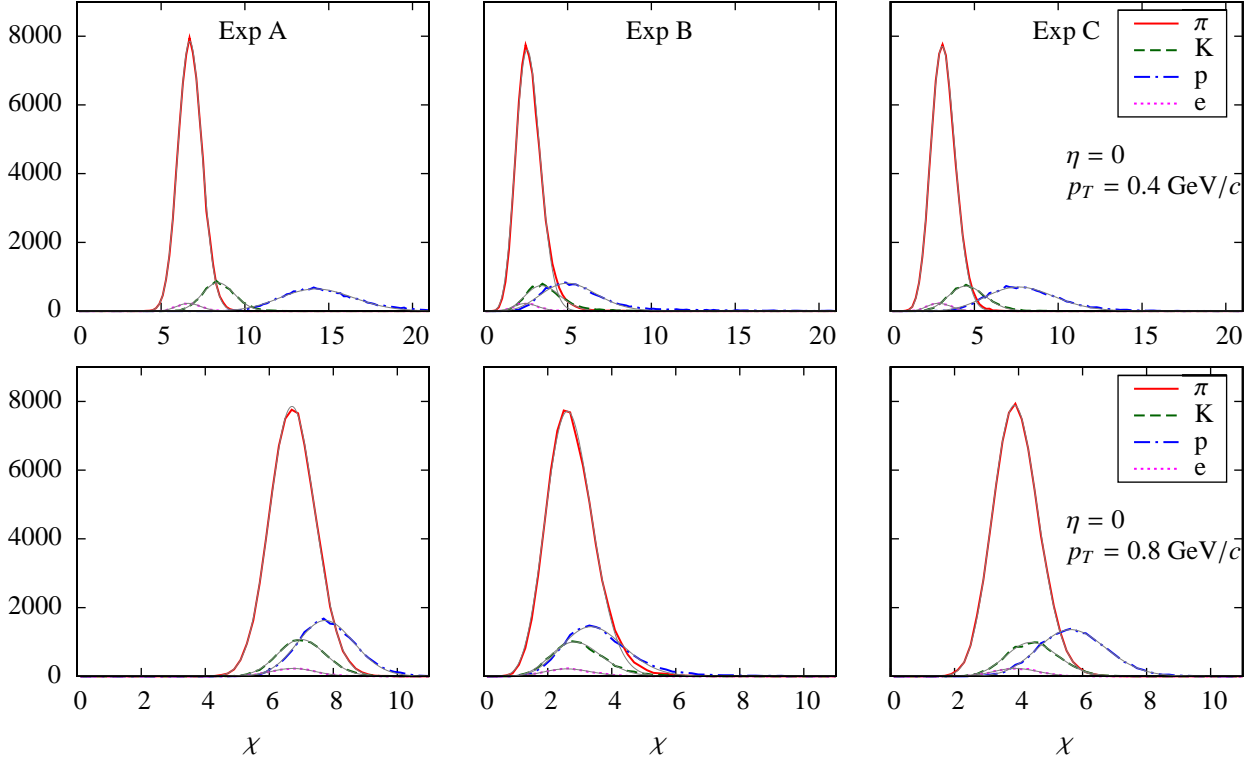


Figure 3: Distributions of  $\chi$  for several particle species. The relative yield of particles was set to  $\pi : K : p : e = 70 : 10 : 18 : 2$ . Results are shown for  $\eta = 0, p_T = 0.4 \text{ GeV}/c$  (upper row) and  $\eta = 0, p_T = 0.8 \text{ GeV}/c$  (lower row) with setups Exp A, B and C. Individual fits with chi distributions are indicated by thin solid lines.

approach to the beam line. The track fitting was performed by a classical Kalman filter [2] with pion mass assumption. The state vector  $x = (\kappa, \theta, \psi, r\phi, z)$  is five dimensional, where

$$\begin{aligned}
 \kappa &= q/p && \text{(signed inverse momentum)} \\
 \theta &= \theta(\vec{p}) && \text{(local polar angle)} \\
 \psi &= \phi(\vec{p}) && \text{(local azimuthal angle)} \\
 r\phi &= r\phi(\vec{r}) && \text{(global azimuthal position)} \\
 z &= r_L && \text{(global longitudinal position)}.
 \end{aligned}$$

The propagation from layer to layer was calculated analytically using a helix model. Multiple scattering and energy loss in tracker layers was implemented with their Gaussian approximations shown in Eqs. (6)–(8). The propagation matrix  $F = \partial f / \partial x$  was obtained by numerical derivation. The measurement vector  $m = (r\phi, z)$  is two dimensional, the measurement operator is

$$H = \begin{pmatrix} 0 & 0 & 0 & 1 & 0 \\ 0 & 0 & 0 & 0 & 1 \end{pmatrix}.$$

The covariance of the process noise  $Q$  is

$$Q = (F_\kappa \otimes F_\kappa^T) \sigma_\kappa^2 + (F_\theta \otimes F_\theta^T) \sigma_\theta^2 + (F_\psi \otimes F_\psi^T) \sigma_\psi^2$$

where  $\sigma_\kappa = \kappa \sigma_\Delta / \beta$ ,  $\sigma_\theta = \sigma_\psi = \theta_0$  and  $F_a = \partial f / \partial x_a$  is a vector. The covariance of measurement noise  $V$  is

$$V = \begin{pmatrix} \sigma_{r\phi}^2 & 0 \\ 0 & \sigma_z^2 \end{pmatrix}$$

Note that multiple scattering contributes equally to the variation of  $\theta$  and  $\psi$ , while energy loss affects only  $\kappa$ .

### 5.1. Results

In order to study the performance of  $\chi$ , charged pions, kaons, protons and electrons with random azimuthal angle were generated and emitted normal to the line of the colliding beams ( $\eta = 0$ ) and run through the above outlined reconstruction.

Distributions of  $\chi$  using  $10^5$  particle tracks are shown in Fig. 3 for  $p_T = 0.4$  and  $0.8$  GeV/ $c$ . For a realistic particle composition the relative yields were set to  $\pi : K : p : e = 70 : 10 : 18 : 2$ . At  $p_T = 0.4$  GeV/ $c$ , in case of Exp A, the protons are detached, but there is a good  $\pi$ - $p$  separation for Exp B and C, as well. For Exp A and C the  $\pi$ - $K$  separation allows for yield estimation. Even at  $p_T = 0.8$  GeV/ $c$  the observed resolution is enough to extract the protons. When fitting the histograms a sum of chi distributions was employed (thin solid lines), but a sum of Gaussians may also be sufficient.

For a complete picture charged pions, kaons, protons and electrons with transverse momenta  $p_T = 0.2, 0.4, 0.6, \dots, 2.0$  GeV/ $c$  and  $\eta = 0$  were used, amounting to  $10^4$  particles per  $p_T$  setting for each particle type and experimental setup. The performance of  $\chi$  as function of  $p$  for all three setups is shown in Fig. 4. The subsequent rows give the dependence of the measured rescaler  $\alpha$ , the fitted number of degrees of freedom  $r$ , the merit function of the histogram fit with sum of chi distributions  $\chi_{fig}^2$  and the separation power  $\rho_\chi$ . This latter was calculated by using the measured  $\alpha$  and  $r$  values with help of Eqs. (3)–(4). The measured values are shown by the symbols. In case of  $\alpha$  the line gives the plain  $\beta(m_0)/\beta(m)$  scaling (Eq. (9)) that works rather well for all three setups and for all particle types. For  $r$  the horizontal lines show the number of split measurements for a given  $p_T$ , decreased by the number of track parameters  $n_p$ . While these predictions are closely followed by the measured values in case of Exp C, there are substantial deviations with the other two setups. It can be traced back to low sensitivity measurements: large number of straw tubes with  $\zeta_{r\phi} = 10$  (Exp A), and two strip layers with  $\zeta_z = 7$  (Exp B). In case of the separation power  $\rho_\chi$  the lines show the approximation based on the predicted number of degrees of freedom and the ratio  $\beta(m)/\beta(m_0)$ , calculated with help of Eq. (10). The steps are due to the changing number of crossed detector layers with varying  $p$ . The approximation works well for Exp C, but strongly overestimates the measured value for Exp A. It is again due to the large number of low sensitivity measurements.

Comparison of the  $\pi$ - $p$  separation power of the  $\chi$  measurement for several experimental setups as a function of momentum is shown in Fig. 5. While Exp A clearly performs better for  $p < 0.6$  GeV/ $c$ , Exp C has better resolution for the more critical higher momentum region. With the most sensitive setups (Exp A and C) protons are  $1\sigma$  apart if  $p < 1.4$  GeV/ $c$ , while  $2\sigma$  separation is reached if  $p < 1$  GeV/ $c$ . For kaons these numbers are  $p < 0.9$  and  $0.5$  GeV/ $c$ , respectively.

## 6. Conclusions

It was shown that tracker detectors can be employed to identify charged particles based on their global  $\chi$  obtained during track fitting with the Kalman filter. This approach builds upon the knowledge of detector material and local position resolution, using the known physics of multiple scattering and energy loss. The study using simplified models of present LHC experiment shows that  $\pi$ - $K$  and  $\pi$ - $p$  unfolding is possible at low momentum. The separation is better than  $1\sigma$  for  $p < 0.9$  and  $1.4$  GeV/ $c$ , respectively. In general, the performance of an experiment is determined by the number of good sensitivity split measurements. It is also a strong function of particle momentum.

If particles can be identified based on informations from other sources (e.g. independent  $dE/dx$  measurement) this tool can still be useful to provide corrections to the amount of material in the detector and to check the obtained precision of its alignment.

## Acknowledgements

The author wishes to thank to Krisztián Krajczár for helpful discussions. This work was supported by the Hungarian Scientific Research Fund and the National Office for Research and Technology (K 48898, H07-B 74296).

## A. Properties of some distributions

In this section the definitions of some used distributions are listed along with their calculated or approximated values for the mean  $\mu$  and variance  $\sigma^2$ .

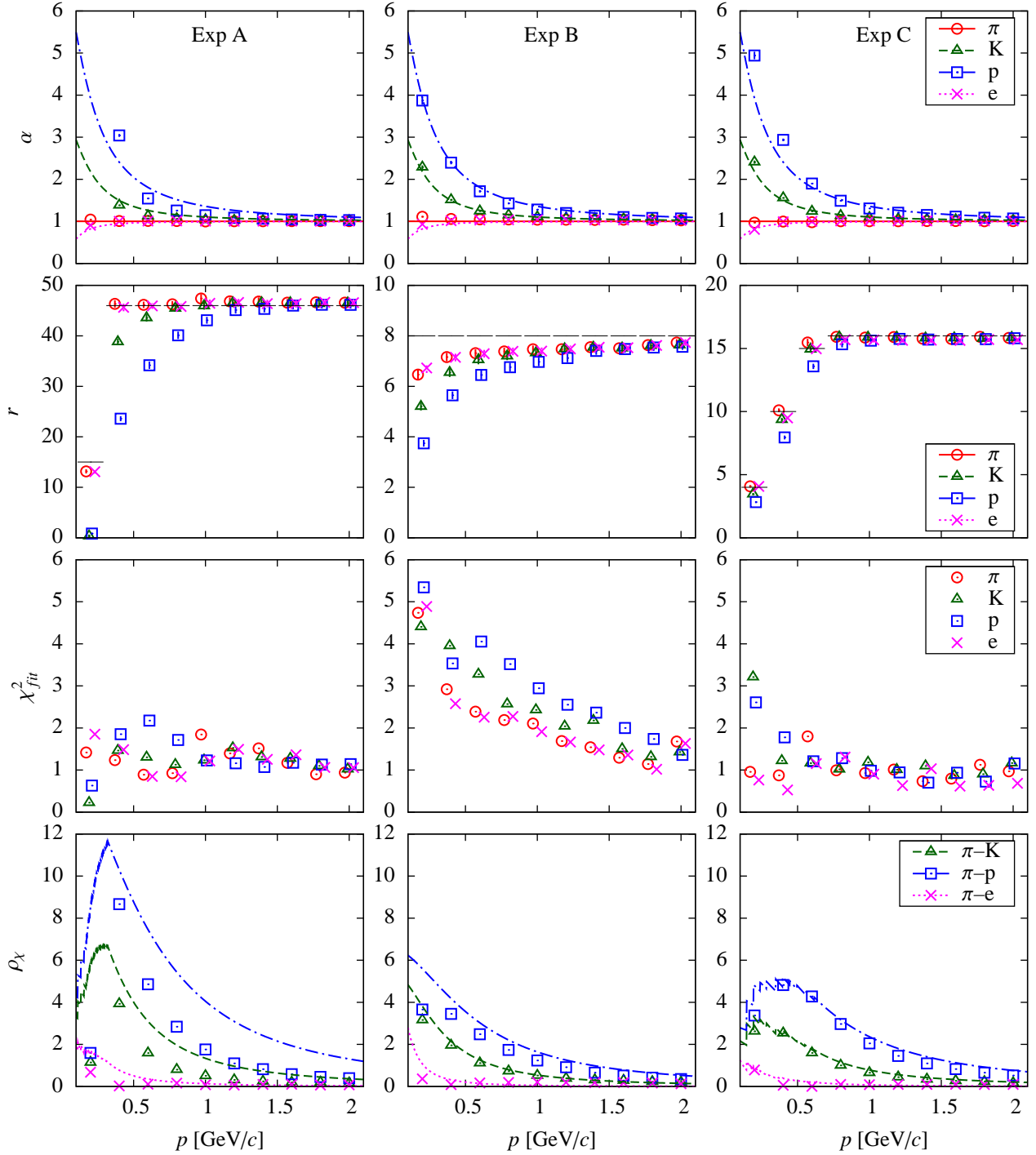


Figure 4: Performance of  $\chi$  measurement for particle identification, with setups Exp A, B and C. For details see text in Sec. 5.1.

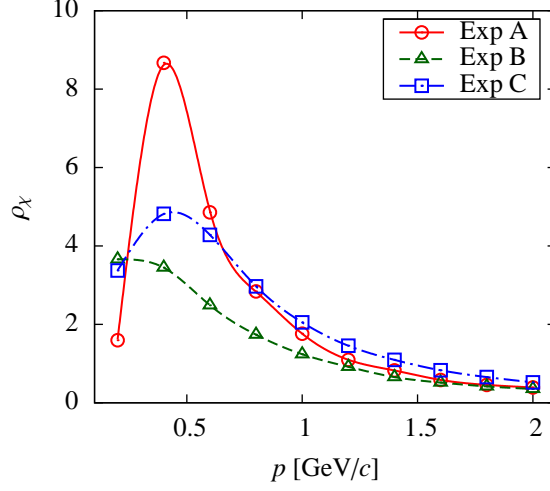


Figure 5: The  $\pi$ - $p$  separation power of the  $\chi$  measurement for the experimental setups, as a function of momentum. The lines are drawn to guide the eye.

### A.1. $\chi^2$ distribution

The distribution, mean and variance are

$$P(x; r) = \frac{x^{r/2-1} e^{-x/2}}{\Gamma\left(\frac{r}{2}\right) 2^{r/2}}$$

$$\mu = r, \quad \sigma^2 = 2r.$$

### A.2. Non-central $\chi^2$ distribution

The distribution, mean and variance are

$$P(x; r, \lambda) = \frac{e^{-(x+\lambda)/2} x^{(r-1)/2} \sqrt{\lambda}}{2(\lambda x)^{r/4}} I_{r/2-1}(\sqrt{\lambda x})$$

$$\mu = r + \lambda, \quad \sigma^2 = 2(r + 2\lambda).$$

where  $I_n(x)$  is the modified Bessel function of the first kind.

### A.3. $\chi$ distribution

The distribution and mean are

$$P(x; r) = \frac{2^{1-n/2} x^{n-1} e^{-x^2/2}}{\Gamma\left(\frac{n}{2}\right)} \quad (11)$$

$$\mu = \frac{\sqrt{2} \Gamma\left(\frac{r+1}{2}\right)}{\Gamma\left(\frac{r}{2}\right)} = \sqrt{r} \left[ 1 - \frac{1}{4r} + \mathcal{O}\left(\frac{1}{r^2}\right) \right] \approx \sqrt{r - \frac{1}{2}} \quad (12)$$

where Ref. [11] for  $r \gg 1$  was used. The variance is

$$\sigma^2 = r - \mu^2 \approx \frac{1}{2}. \quad (13)$$

#### A.4. Non-central $\chi$ distribution

The distribution and mean are

$$P(x; r, \lambda) = \frac{e^{-(x^2+\lambda^2)/2} x^r \lambda}{(\lambda x)^{r/2}} I_{r/2-1}(\lambda x)$$

$$\mu = \sqrt{\frac{\pi}{2}} L_{1/2}^{(r/2-1)}\left(\frac{-\lambda^2}{2}\right)$$

where  $L_n^{(a)}(x)$  is the generalized Laguerre function. For  $r \gg 1$ , with Kummer's second formula [12]

$$\mu = \sqrt{\frac{\pi}{2}} \frac{\Gamma\left(\frac{r+1}{2}\right)}{\Gamma\left(\frac{r}{2}\right)\Gamma\left(\frac{3}{2}\right)} {}_1F_1\left(-\frac{1}{2}, \frac{r}{2}, \frac{-\lambda^2}{2}\right)$$

where  ${}_1F_1(a, b, z)$  is the confluent hypergeometric function of the first kind. With help of Eq. (12) and Ref. [13], assuming  $\lambda^2 \ll r$

$$\mu = \sqrt{r} \left[ 1 - \frac{1}{4r} + \mathcal{O}\left(\frac{1}{r^2}\right) \right] \left[ 1 + \frac{\lambda^2}{2r} + \mathcal{O}\left(\frac{1}{r^2}\right) \right] \approx$$

$$\approx \sqrt{r} \left[ 1 - \frac{1-2\lambda^2}{4r} + \mathcal{O}\left(\frac{1}{r^2}\right) \right] \approx \sqrt{r - \frac{1}{2} + \lambda^2}. \quad (14)$$

For the variance

$$\sigma^2 = r - \mu^2 + \lambda^2 \approx \frac{1}{2}. \quad (15)$$

Note that with  $\lambda = 0$  we get back the mean of the  $\chi$  distribution (Eqs. (12) and (14)), while the variances are the same in the central and non-central case (Eqs. (13) and (15)).

## B. Sum of non-central chi-squared distributed independent variables

The goal is to approximate the sum

$$y = \sum_{i=1}^n a_i z_i$$

where  $z_i$  are non-central chi-squared distributed independent random variables with one degree of freedom and density function  $f_X(z_i; 1, \lambda_i)$ . Although an explicit expression for the distribution of  $y$  exists, it is difficult to evaluate in practice [14]. Here this function is approximated by a rescaled non-central chi-squared distribution  $1/\alpha f_X(x/\alpha; r, \lambda)$  by requiring that the first two moments be the same. The means and variances are additive, thus the equations two solve are

$$\langle y \rangle = \sum_i a_i (1 + \lambda_i) = \alpha (r + \lambda)$$

$$\langle (y - \langle y \rangle)^2 \rangle = 2 \sum_i a_i^2 (1 + 2\lambda_i) = 2\alpha^2 (r + 2\lambda)$$

By assuming  $\lambda_i \ll 1$  we get

$$\alpha = \frac{\sum_i a_i^2}{\sum_i a_i}, \quad r = \frac{(\sum_i a_i)^2}{\sum_i a_i^2}, \quad \lambda = \sum_i \lambda_i$$

with relative corrections of the order  $\mathcal{O}(\lambda^2/r^2)$ . If the values of  $a_i$  are similar some of the above expressions can be approximated by

$$\alpha \approx \langle a_i \rangle, \quad r \approx n.$$

## References

- [1] A. Grossheim, K. Zuber, Momentum determination via multiple scattering in AQUA- RICH, Nucl. Instrum. Meth. A533 (2004) 532–542. doi:10.1016/j.nima.2004.06.146.
- [2] R. Fruhwirth, Application of Kalman filtering to track and vertex fitting, Nucl. Instrum. Meth. A262 (1987) 444–450. doi:10.1016/0168-9002(87)90887-4.
- [3] A. Ankowski, et al., Measurement of through-going particle momentum by means of multiple scattering with the ICARUS T600 TPC, Eur. Phys. J. C48 (2006) 667–676. doi:10.1140/epjc/s10052-006-0051-3.
- [4] W. Hulsbergen, The global covariance matrix of tracks fitted with a Kalman filter and an application in detector alignment, Nucl. Instrum. Meth. A600 (2009) 471–477. arXiv:0810.2241, doi:10.1016/j.nima.2008.11.094.
- [5] C. Amsler, et al., Review of particle physics, Phys. Lett. B667 (2008) 1. doi:10.1016/j.physletb.2008.07.018.
- [6] H. Bichsel, Straggling in thin silicon detectors, Rev. Mod. Phys. 60 (1988) 663–699. doi:10.1103/RevModPhys.60.663.
- [7] G. Aad, et al., Expected Performance of the ATLAS Experiment - Detector, Trigger and Physics (2009). arXiv:0901.0512.
- [8] F. Antinori, The Alice inner tracking system, Nucl. Instrum. Meth. A511 (2003) 215–220. doi:10.1016/S0168-9002(03)01796-0.
- [9] D. Antonczyk, et al., Performance studies with an ALICE TPC prototype, Nucl. Instrum. Meth. A565 (2006) 551–560. doi:10.1016/j.nima.2006.06.022.
- [10] R. Adolphi, et al., The CMS experiment at the CERN LHC, JINST 3 (2008) S08004. doi:10.1088/1748-0221/3/08/S08004.
- [11] R. L. Graham, D. E. Knuth, O. Patashnik, Concrete Mathematics: A Foundation for Computer Science, 2nd Edition, Addison-Wesley, Reading, MA, 1994, answer to Problem 9.60.
- [12] W. Koepf, Hypergeometric Summation: An Algorithmic Approach to Summation and Special Function Identities, Vieweg, Braunschweig, Germany, 1998.
- [13] M. Abramowitz, I. A. Stegun, Handbook of Mathematical Functions with Formulas, Graphs, and Mathematical Tables, Dover, New York, 1972.
- [14] S. Gabler, C. Wolff, A quick and easy approximation to the distribution of a sum of weighted chi-square variables, Statistical Papers 28 (1) (1987) 317–325. doi:10.1007/BF02932611.